



Cite this: *Biomater. Sci.*, 2020, **8**, 1148

## Tannic acid-based nanogel as an efficient anti-inflammatory agent†

Jiwon Yeo,‡ Junseok Lee,  ‡ Seonyeong Yoon and Won Jong Kim  \*

Biologically produced reactive oxygen species (ROS) are important signaling molecules in the human body. Despite their importance under normal conditions, abnormal overproduction of ROS under unbalanced or irregular homeostasis can cause severe inflammatory diseases. Various antioxidants have been developed in the biomedical field to resolve high levels of ROS; however, high doses of natural antioxidants such as polyphenol can induce side effects on health. Further, synthetic antioxidants are still controversial in regards to their safety and their complicated synthesis. Inspired from our previous work, a nitric oxide-scavenging nanogel designed for treating rheumatoid arthritis, we report herein a biocompatible tannic acid (TA)-based nanogel as an effective ROS scavenger. A polymeric phenylboronic acid-tannic acid nanogel (PTNG) was prepared by simply mixing through to the formation of phenylboronic ester bonds between polymeric phenylboronate and TA. We focused on the reaction of phenylboronic ester with H<sub>2</sub>O<sub>2</sub>, which readily consumes H<sub>2</sub>O<sub>2</sub> molecules, and applied it as an antioxidant. In addition, TA is a well-known antioxidant, specifically a free radical scavenger; thus, we expected combinatory ROS scavenging effects for PTNG. Various ROS scavenging assays revealed the significant antioxidant effects of PTNG. Under an induced inflammation model *in vitro*, our PTNG showed high biocompatibility as well as strong anti-inflammatory effects. Furthermore, in the zymosan-induced peritonitis mouse model, a representative acute inflammation model *in vivo*, PTNG reduced significant neutrophil recruitment and pro-inflammatory cytokines, indicating successful alleviation of inflammation. On the basis of these results, we suggest that PTNG has great potential as an antioxidant and should find application in the treatment of further ROS-overproducing inflammatory diseases.

Received 29th August 2019,  
Accepted 19th October 2019

DOI: 10.1039/c9bm01384a

rsc.li/biomaterials-science

### 1. Introduction

Reactive oxygen species (ROS) are highly reactive molecules containing at least one oxygen atom, produced from the mitochondrial electron transport chain or from NADPH oxidase on the plasma membrane. Several ROS, including hydrogen peroxide (H<sub>2</sub>O<sub>2</sub>), the hydroxyl radical (OH<sup>•</sup>), and the superoxide anion (O<sub>2</sub><sup>•-</sup>) are used as signaling molecules, thus they are necessary to maintain metabolism and cellular functions such as cell proliferation, differentiation,<sup>1</sup> signal transduction,<sup>2</sup> pathogen defense,<sup>3</sup> and regulation of inflammation.<sup>4</sup> In normal physiological conditions, the formation and elimination of ROS is well balanced by intrinsic antioxidants. When the balance of ROS is broken through a deficiency of antioxidants or mutation of ROS-producing systems, however, abnor-

mally overproduced ROS cause pathologically deleterious effects on humans by impairing proteins, lipids, and DNA. In particular, many reports have revealed that overproduction of ROS is strongly correlated with chronic inflammatory diseases, including rheumatoid arthritis,<sup>5</sup> atherosclerosis,<sup>6</sup> stroke,<sup>7</sup> cancer,<sup>8</sup> *etc.* Hence, scavenging abnormally produced ROS can be considered to be one of the alternative methods for treating inflammatory diseases.

Natural antioxidants including polyphenol, carotenoids, vitamin E and vitamin C draw great attention in antioxidant therapy thanks to their significant biological functions such as anti-inflammatory effects, as well as antibacterial effects and anti-aging effects. However, high doses of natural antioxidants are required to achieve a therapeutic effect, and this might cause harmful effects on health.<sup>9–14</sup> Therefore, several synthetic antioxidants have also been studied in order to enhance antioxidant effects in moderate doses. In that perspective, ROS-scavenging nanoparticles (ROS-SNPs) have recently been developed in order to investigate their antioxidant effects as well as their potential further application in the treatment of inflammatory disorders. For instance, metal oxide-based ROS-SNPs such as cerium oxide (CeO<sub>2</sub>) and manganese oxide

Department of Chemistry, Pohang University of Science and Technology (POSTECH), Pohang 37673, Republic of Korea. E-mail: wjkim@postech.ac.kr;

Fax: +82-54-279-3399; Tel: +82-54-279-2104

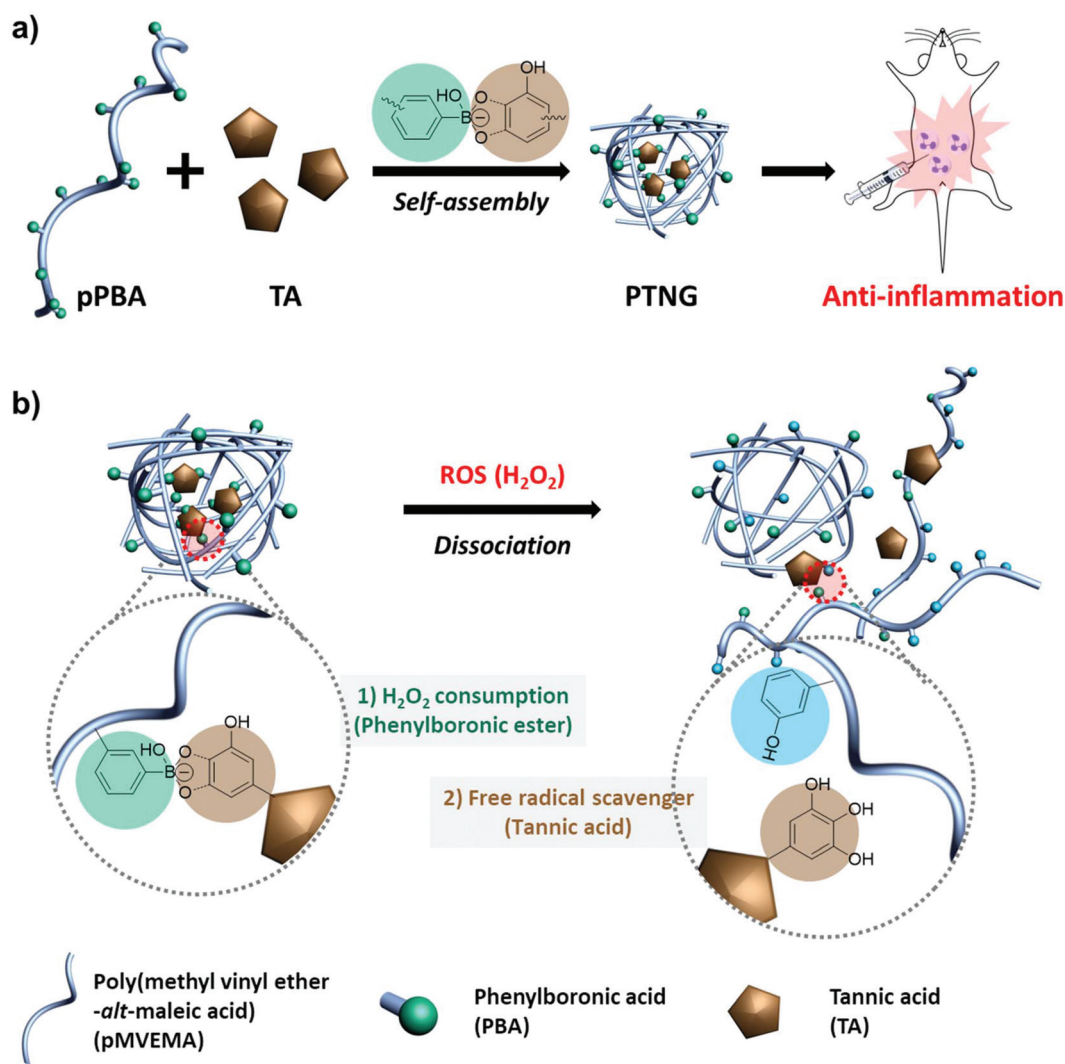
†Electronic supplementary information (ESI) available. See DOI: 10.1039/c9bm01384a

‡These authors contributed equally to this work.

( $\text{Mn}_3\text{O}_4$ ) have recently been developed. Based on the ROS-scavenging ability of cerium oxide from the chemical balance between  $\text{Ce}^{3+}$  (reduced state) to  $\text{Ce}^{4+}$  (oxidized state). Kwon *et al.* proposed mitochondria targeting cerium oxide nanoparticles for treating Alzheimer's disease.<sup>15</sup> Yao *et al.* reported that manganese oxide nanoparticles can eliminate ROS even more effectively than cerium oxide, and is more stable than other natural antioxidants.<sup>16</sup> Although several metal oxides exhibit great ROS-scavenging ability, there is concern regarding low biocompatibility and potential toxicity.<sup>17–20</sup> Another interesting strategy for eliminating ROS based on natural products has been reported. The  $\beta$ -cyclodextrin-based, nanoparticle-harnessing, and ROS-responsive phenylboronic acid pinacol ester group was developed by Zhang *et al.*<sup>21</sup> It showed good antioxidant and anti-inflammatory effects *in vitro*, and biomedical application of it as an anti-inflammatory agent was proposed. Despite the above advantages, an immediate application might be impeded by complex and difficult synthetic pro-

cedures. Therefore, a ROS-scavenging system showing good biocompatibility, facile preparation, and a strong ROS-eliminating capability would be a proper candidate for use as an alternative anti-inflammatory agent.

Recently our group reported polymeric phenylboronate (pPBA) and its biomedical application as drug delivery system.<sup>22</sup> It was simply synthesized by a spontaneous ring-opening reaction with poly(maleic anhydride) and grafted PBA moiety on a polymer backbone that could form phenylboronic ester by binding with 1,2- or 1,3-diol and catechol groups. Inspired by our previous work, we focused on natural antioxidants having catechol groups for easy formulation of a ROS-scavenging phenylboronic ester. Among the natural antioxidants, tannic acid (TA) has 10 catechol or gallol groups per molecule and possesses innate free-radical scavenging effects derived from the catechol groups, thus many reports have highlighted the potential of TA as an antioxidant, anti-carcinogen, and anti-inflammation agent.<sup>23–25</sup> Accordingly, we devel-



**Scheme 1** (a) Preparation and administration of self-assembled PTNG and (b) illustration of combinatorial ROS-scavenging effects of PTNG; the phenylboronic ester bond consumes  $\text{H}_2\text{O}_2$ , and TA scavenges the free radical, respectively.

oped a biocompatible antioxidant nanoparticle with an easy synthetic method. By simple mixing of pPBA and TA, a self-assembled pPBA-TA nanogel (PTNG) was prepared through interaction between grafted PBA moieties and catechol groups in TA. The phenylboronic ester group in PTNG is readily broken by  $\text{H}_2\text{O}_2$  to release TA, which means consuming  $\text{H}_2\text{O}_2$  under degradation. Furthermore, released TA is also a strong free radical scavenger, thus we expected that PTNG would show synergistic ROS-scavenging effects from phenylboronic ester groups and released TA, resulting in greatly enhanced anti-inflammatory effects *in vitro* and *in vivo* (Scheme 1).

## 2. Materials and methods

### 2.1 Reagents

Hydrogen peroxide (34.5%  $\text{H}_2\text{O}_2$ ) solution was purchased from Samchun, Korea. Tannic acid, poly(methyl vinyl ether-*alt*-maleic anhydride) (pMVEMA,  $M_n \sim 80\,000\text{ g mol}^{-1}$ ), 3-aminophenylboronic acid (PBA-NH<sub>2</sub>) monohydrate, phorbol 12-myristate 13-acetate (PMA), zymosan A from *Saccharomyces cerevisiae*, lipopolysaccharide (LPS), and thiazolyl blue tetrazolium bromide (MTT) were purchased from Sigma (St Louis, MO). Dulbecco's modified Eagle's medium (DMEM) and fetal bovine serum (FBS) were purchased from Capricorn scientific (Ebsdorfergrund, Germany). Modified Eagle's medium alpha (MEM- $\alpha$ ), an Amplex® Red hydrogen peroxide/peroxidase assay kit, and antibodies for flow cytometry (PE-Cy5 anti-mouse F4/80, PE anti-mouse CD11b, and FITC anti-mouse Ly6G) were purchased from Thermo Fisher Scientific (Carlsbad, CA). ROS-Glo  $\text{H}_2\text{O}_2$  assay was purchased from Promega (Madison, WI). A myeloperoxidase (MPO) assay kit and a DCFDA cellular ROS assay kit were purchased from Abcam (Cambridge, MA). ELISA kits for mouse IL-6 and TNF- $\alpha$  were purchased from Koma Biotech (Korea). CT-26 (murine colon cancer) and RAW 264.7 (murine macrophage) cell lines were purchased from Korean Cell Line Bank (Korea).

### 2.2 Instrumental methods

Absorbance and fluorescence for the ROS assay, ELISA, and MTT assay were measured by a multi-mode microplate reader (SpectraMax® i3, Molecular Devices) and analyzed by the SoftMax® Pro 6 software. Fluorescence microscope images were obtained using a Nikon Eclipse Ti-E and were analyzed with NIS-Elements software (ver. 4.2). Confocal laser scanning microscope (CLSM) images were obtained using an Olympus FV-3300 and were analyzed using OLYMPUS FLUOVIEW Viewer (ver. 1.7). Flow cytometry was performed using a cell analyzer (FACSCalibur, Becton Dickinson) and the data was analyzed using BD CellQuest software. All obtained data were statistically analyzed by GraphPad Prism 7.

### 2.3 Synthesis of polymeric phenylboronate (pPBA)

We synthesized polymeric phenylboronate (pPBA) by grafting PBA-NH<sub>2</sub> onto a poly(maleic anhydride) backbone (pMVEMA), following our previously reported method. First, PBA-NH<sub>2</sub>

(320 mg, 2 mmol) and poly(methyl vinyl ether-*alt*-maleic anhydride) (1 g, 6.4 mmol) were dissolved in dry dimethyl sulfoxide (DMSO), and the PBA-NH<sub>2</sub> solution was added to the pMVEMA solution to initiate the spontaneous ring opening reaction. After 24 h, NaOH was added into the reaction mixture to hydrolyze any remaining succinic anhydride moiety, followed by dialysis with deionized water for 3 days (MWCO = 10 kDa) and lyophilization. The conjugated PBA molar ratio was calculated by <sup>1</sup>H NMR (yield: 80%).

<sup>1</sup>H NMR ( $\text{D}_2\text{O}$ , 300 MHz): 7.7–7.0 (m, Ph, 4H); 3.8–3.5 (m, –CH–, 1H); 3.5–3.1 (m, –OCH<sub>3</sub>, 3H); 3.1–2.4 (m, anhydride, 2H); 2.4–1.4 (m, –CH<sub>2</sub>–, 2H).

### 2.4 Synthesis of polymeric phenylboronate-tannic acid nanogel

Formation of the PTNG was carried out by simple mixing of pPBA and TA solutions at the desired ratio. In detail, PTNG was formulated with molar ratios of [PBA]:[TA] from 50:1 to 1:1 by mixing 100 mM [PBA] and the corresponding volume of 10 mM [TA], followed by the addition of 10× glycine-NaOH buffer (pH 8.5), with the balance filled by DW. [PBA]:[TA] = 10:1 PTNG was used for further studies. From this point on, the concentration of PTNG will be regarded as its [PBA] equivalent. For binding assay between PBA and TA, 1 mM [PBA] was used, varying with the amount of [TA]. Fluorescence spectra of [PBA] were measured at  $\lambda_{\text{ex}} = 388\text{ nm}$ .

### 2.5 Assessment of ROS-responsive and scavenging properties of PTNG

For evaluation of ROS-responsive properties, 100  $\mu\text{M}$  [PBA] of PTNG was incubated in 100  $\mu\text{M}$   $\text{H}_2\text{O}_2$  for 2 h, and hydrodynamic size was measured by DLS. A transmission electron microscope (TEM) image was obtained at 24 h after adding 100  $\mu\text{M}$   $\text{H}_2\text{O}_2$  into the PTNG solution.

Free-radical scavenging ability was measured by DPPH assay. In brief, pPBA, TA, or PTNG corresponding to 100  $\mu\text{M}$  [PBA] equivalence were added into 500  $\mu\text{M}$  DPPH in EtOH solution and incubated in darkness for 15 min. Absorbance of the remaining DPPH was measured at 517 nm, and that of non-treated DPPH was regarded as 100%.

For assessment of  $\text{H}_2\text{O}_2$  scavenging ability, commercially available chemiluminescence-based ROS-Glo™  $\text{H}_2\text{O}_2$  assay was used as a non-HRP-based assay. 200  $\mu\text{M}$   $\text{H}_2\text{O}_2$  was added to samples including pPBA, TA, or PTNG corresponding to 100  $\mu\text{M}$  [PBA] equivalence and incubated at room temperature (RT) for 2 h. From this point, we proceeded following the manufacturer's protocols.

The HRP-based assay was regarded as a total ROS assay, and we used Amplex Red®  $\text{H}_2\text{O}_2$  assay. Similarly, 200  $\mu\text{M}$   $\text{H}_2\text{O}_2$  was added into samples including pPBA, TA, or PTNG corresponding to 100  $\mu\text{M}$  [PBA] equivalence and incubated for 2 h at RT. The next step was conducted following the manufacturer's protocols.

### 2.5 Cell viability

Cytotoxicity after treatment of pPBA, TA, and PTNG were evaluated dose-dependently against mouse colon cancer cell line

(CT-26) and macrophage cell line (RAW 264.7). Briefly, cells were seeded on a 96-well plate at a density of 8000 cells per well for CT-26, and at 10 000 cells per well for RAW 264.7, in DMEM and incubated overnight. The medium was replaced by 200  $\mu\text{L}$  of fresh MEM- $\alpha$ , 200  $\text{ng mL}^{-1}$  of PMA in-medium, or 200  $\mu\text{M}$  of  $\text{H}_2\text{O}_2$  in-medium, then pPBA, TA, or PTNG corresponding to 0–200  $\mu\text{M}$  [PBA] equivalence was added. After incubation for 24 h, viability of residual cells was evaluated by MTT assay. For evaluation of toxicity of PMA and  $\text{H}_2\text{O}_2$ , RAW 264.7 cells were cultured with either 0–1000  $\text{ng mL}^{-1}$  PMA or 0–1000  $\mu\text{M}$   $\text{H}_2\text{O}_2$  for 24 h, and viability was evaluated by MTT assay.

For the MTT assay, the medium was replaced by the addition of 200  $\mu\text{L}$  of 0.5  $\text{mg mL}^{-1}$  of MTT in DMEM, and the solution was further incubated in darkness for 4 h. The medium was carefully discarded, and the residual crystals were fully dissolved by 100  $\mu\text{L}$  of DMSO. Absorbance was measured at 570 nm, and the relative absorbance of non-treated cells was regarded as 100% viability. The ROS protection rate was calculated by the following: Protection rate (%) =  $100 \times (\text{viability}_{\text{ROS+sample}} - \text{viability}_{\text{ROS}}) / (\text{viability}_{\text{non-treat}} - \text{viability}_{\text{ROS}})$ .

## 2.6 Extracellular ROS and extracellular pro-inflammatory cytokine level

In order to demonstrate the ROS-scavenging effect at the cellular level, extracellular level of ROS, and pro-inflammatory cytokine (IL-6 and TNF- $\alpha$ ) after treatment of pPBA, TA, and PTNG were evaluated dose-dependently against RAW 264.7 after activation with either 200  $\text{ng mL}^{-1}$  PMA or 200  $\mu\text{M}$   $\text{H}_2\text{O}_2$ . Briefly, cells were seeded on a 12-well plate at a density of 200 000 cells per well and incubated overnight. The medium was replaced by 1 mL of fresh MEM- $\alpha$ , MEM- $\alpha$  with 200  $\text{ng mL}^{-1}$  of PMA, or 200  $\mu\text{M}$  of  $\text{H}_2\text{O}_2$ , and with the addition of pPBA, TA, or PTNG corresponding to 0–200  $\mu\text{M}$  [PBA] equivalence. After incubation for 24 h, the medium was carefully collected and centrifuged (3000 rpm, 10 min) to discard dead cells and debris from the medium. The supernatant was carefully transferred into a 96-well plate for quantification of whole ROS by Amplex® Red ROS assay, and cytokines by ELISA. For all assays, the protocol of the manufacturer was carefully followed. Fluorescence at 560/590 nm and absorbance at 450 nm were measured for the Amplex® Red ROS assay and ELISA, respectively.

## 2.7 Intracellular ROS level by fluorescence microscopy

Intracellular ROS level was determined by ROS-responsive DCF-DA. Briefly, RAW 264.7 cells were seeded on the 6-well confocal plate at a density of 100 000 cells per well and incubated overnight. The medium was replaced by 2 mL of fresh MEM- $\alpha$ , MEM- $\alpha$  with 200  $\text{ng mL}^{-1}$  of PMA, or 200  $\mu\text{M}$  of  $\text{H}_2\text{O}_2$ , and the addition of pPBA, TA, or PTNG corresponding with 0–200  $\mu\text{M}$  [PBA] equivalence. After incubation for 24 h, cells were washed thoroughly and the medium was replaced by fresh DMEM containing 25  $\mu\text{M}$  of DCF-DA. After incubation for 10 min, cells were fixed with 10% MeOH for 5 min and were observed by fluorescence microscopy at FITC channel.

## 2.8 Animal

All experiments involving animals were approved by the POSTECH Biotech Center Ethics Committee (POSTECH-2019-0021) under guidelines and regulations provided by Postech Institutional Animal Care and Use Committee (IACUC). Female BALB/c mice (4-week old,  $16 \pm 2$  g) were supplied from Joong Ah Bio (Suwon, Korea) and housed under optimal lighting, temperature, and humidity, with access to water and food *ad libitum*. An acclimation period of at least 72 h was provided for all mice prior to the performance of any experiment.

## 2.9 Hemolysis assay

Mouse whole blood was obtained from female Balb/c mice and readily diluted 10-fold with PBS. Erythrocytes were collected by centrifugation (2000 rpm, 15 min) and the pellet was re-suspended into 10-fold PBS. Samples (pPBA, pMVEMA, TA, and PTNG) were mixed at a final concentration of corresponding [PBA] = 200  $\mu\text{M}$  and incubated at 37  $^\circ\text{C}$  for 6 h. Then, the remaining erythrocytes were centrifuged (2000 rpm, 15 min) to obtain the hemolysis supernatant, and the absorbance at 541 nm was measured. PBS and a  $1 \times$  lysis buffer were regarded as 0% and 100% hemolysis, respectively.

## 2.10 *In vivo* peritonitis model

In order to induce acute peritonitis, 800  $\mu\text{L}$  of 1  $\text{mg mL}^{-1}$  zymosan was injected i.p., and 200  $\mu\text{L}$  of 200 nmol [PBA] equivalent samples (PBS, pMVEMA, pPBA, TA, or PTNG) were administered i.p. at 1 h. After 5 h, mice were anesthetized and 2 mL of cold PBS was injected into the peritoneum, mice were gently shaken, and peritoneal lavage (>1.5 mL) was collected. Also, whole blood was obtained by heart puncture and serum was separated to measure the cytokine level by ELISA. Extracted peritoneal lavage was centrifuged (400g, 8 min) to separate cells and exudate. Cytokine (IL-6 and TNF- $\alpha$ ) level of the exudate was evaluated by ELISA and MPO activity using a commercially available kit. The pellet was dispersed in ACK lysis buffer to eliminate erythrocytes, the cells were washed and then counted by hemocytometer. Also, cells were re-suspended at a density of  $1 \times 10^7$  cells per mL. For flow cytometry, FcR was blocked, followed by staining with PE-Cy5 anti-mouse F4/80, PE anti-mouse CD11b, and FITC anti-mouse Ly6G for 30 min in darkness. Cells were washed, fixed with 10% NBF, and analyzed by flow cytometry.

# 3. Results and discussion

## 3.1 Formation of pPBA-TA nanogel (PTNG)

We firstly synthesized pPBA, which reacts with the catechol group of TA to form a phenylboronic ester group, by following our previous protocol. In brief, amine-functionalized PBA (PBA-NH<sub>2</sub>) was simply mixed with poly(methyl vinyl ether-*alt*-maleic anhydride) (pMVEMA), the product was purified by dialysis. Successful synthesis of pPBA was confirmed by <sup>1</sup>H NMR and its conjugation ratio was around 30% (Fig. S1a†).<sup>22</sup> Next, we investigated the formation of nanogels by simply mixing pPBA and TA in different molar ratios, and the size of

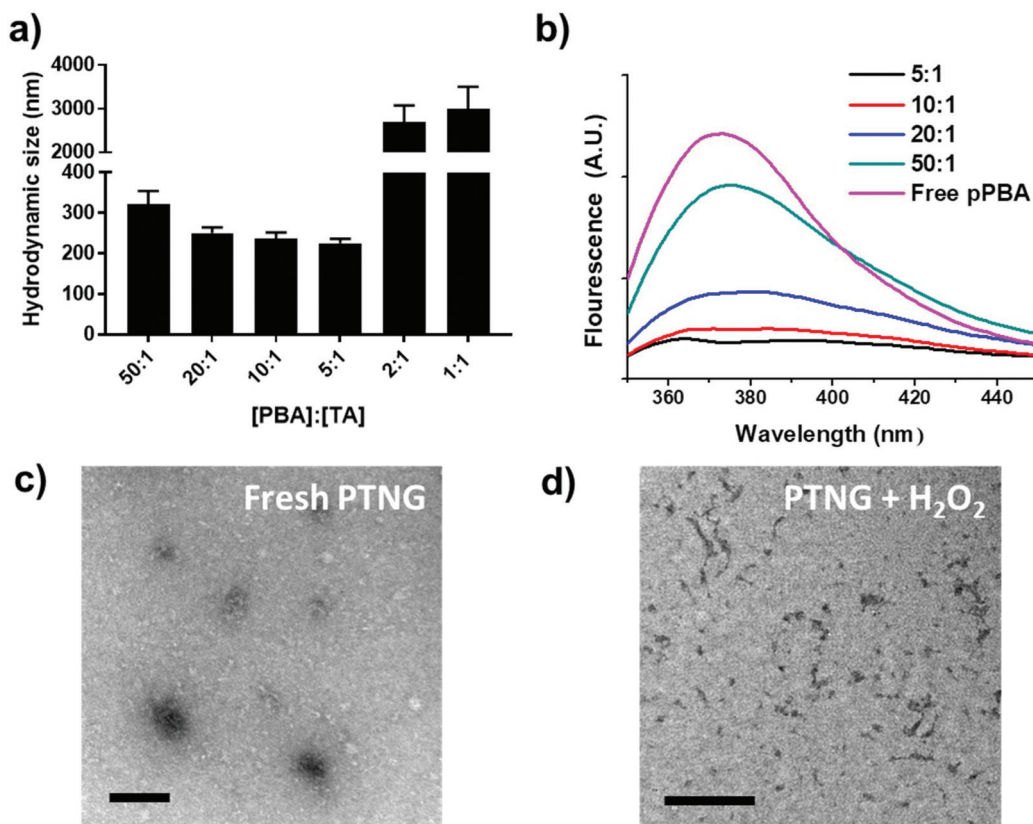


**Fig. 1** Characterization of PTNG. (a) Hydrodynamic size of PTNG and (b) intrinsic fluorescence of PBA varying with the ratio of PBA and TA. TEM image of PTNG (c) without  $\text{H}_2\text{O}_2$  and (d) after treating with  $\text{H}_2\text{O}_2$  (scale bars = 200 nm and 100 nm, respectively).

samples was analyzed by dynamic light scattering (DLS). We postulated that the best ratio of [PBA] to [TA] would be 5 to 1, because only five outer catechol groups of TA might react with the PBA moiety in pPBA, while inner catechol groups may not interact with the PBA moiety due to steric hindrance. Although we observed the most compact size in the ratio of 5 to 1, the distribution of sizes was not clearly uniform (Fig. S1b†). However, compared with the ratio of 5-to-1, the 10-to-1 sample showed a uniform distribution with a particle size of around 250 nm. Furthermore, the size of samples with too high of a TA ratio, such as 2-to-1 or 1-to-1, was over the nanoscale because of intramolecular hydrogen bonding between TAs (Fig. 1a).<sup>26</sup> Hence, we chose the ratio of 10-to-1 as the best condition for further formulation of PTNG. We also performed the binding affinity test to check the interaction between PBA and TA, and observed quenching of the intrinsic PBA fluorescence.<sup>22</sup> Correlated with hydrodynamic size, when the ratio of TA to PBA increased, fluorescence of PBA was reduced, and the ratio of 5-to-1 showed the lowest fluorescence intensity at 380 nm, indicating successful formation of hydrogen peroxide ( $\text{H}_2\text{O}_2$ )-responsive phenylboronic ester (Fig. 1b).

### 3.2 ROS-responsive property and scavenging of pPBA-TA nanogel (PTNG)

Phenylboronic ester is a widely used chemistry in the biomedical field and includes smart delivery<sup>27,28</sup> and probe

systems<sup>29</sup> that exploit the  $\text{H}_2\text{O}_2$ -responsive property. In this study, we observed the  $\text{H}_2\text{O}_2$ -responsive property of PTNG by monitoring the size change by both DLS and TEM. As shown in Fig. 1c, d, and S1b,† while fresh PTNG showed a uniform size distribution and particles maintained their spherical shape at approximately 200 nm in size, a decrease in size and an irregular distribution of size were observed after treatment with  $\text{H}_2\text{O}_2$ . The result verified that the phenylboronic ester bond formation in PTNG was cleaved by  $\text{H}_2\text{O}_2$ , resulting in collapse of the PTNG.

From the result of  $\text{H}_2\text{O}_2$ -responsive disruption of PTNG, we expected it to be a strong ROS scavenger by (1) consuming  $\text{H}_2\text{O}_2$  for degradation of phenylboronic ester and (2) innate ROS scavenging effects of released TA, a well-known antioxidant and free radical scavenger. On the basis of the idea, we investigated ROS-scavenging property of PTNG by total ROS,  $\text{H}_2\text{O}_2$ , and free-radical scavenging assay. First, for evaluating the total ROS level, we used horseradish peroxidase (HRP)-based ROS quantification assay. It is worth noting that although the HRP-based ROS assay is well known for quantification of  $\text{H}_2\text{O}_2$ , actually both  $\text{H}_2\text{O}_2$  as a substrate and  $\text{Fe(IV)}$  oxide radical as an intermediate are involved in the peroxidase cycle.<sup>30</sup> Therefore, we assumed that the  $\text{H}_2\text{O}_2$  and radical are scavenged by phenylboronic ester and TA, respectively, and regarded HRP/ $\text{H}_2\text{O}_2$  assay as the total ROS quantification method. As expected, PTNG significantly reduced the ROS

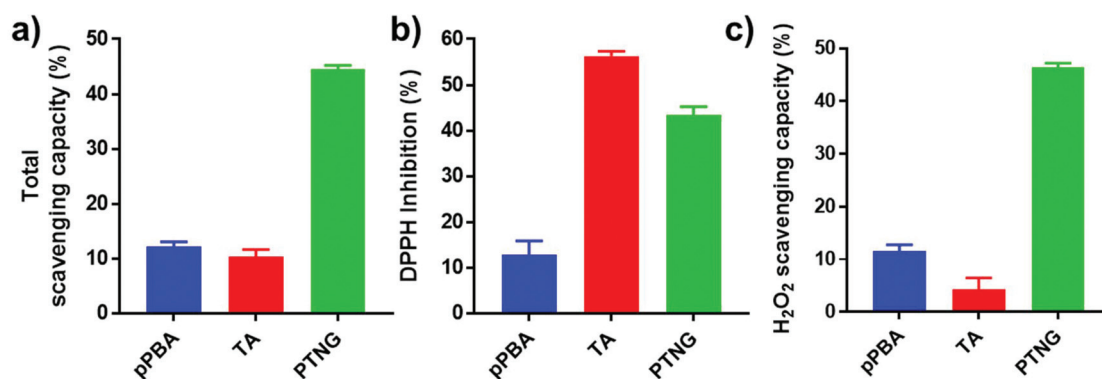


Fig. 2 ROS scavenging ability relating to (a) total ROS, (b) free radical (DPPH), and (c) H<sub>2</sub>O<sub>2</sub> scavenging assay ( $n = 3$ , mean  $\pm$  SD).

level, resulting from combination effects of TA and phenylboronic ester. pPBA and TA also decreased some level of ROS, which is derived from the ROS scavenging nature of phenylboronic acid and catechol, respectively (Fig. 2a). An increase in the ROS-scavenging ability of PTNG with an increase in PTNG concentration was also observed (Fig. S2a<sup>†</sup>). Next, we investigated the free-radical scavenging ability by colorimetric 2,2-diphenyl-1-picrylhydrazyl (DPPH) radical assay. As expected, TA, a well-known antioxidant, showed strong inhibition effects of the DPPH free radical, whereas the effect of pPBA was negligible. Interestingly, PTNG also had a certain level of capability for scavenging free radicals, which might be derived from the remaining catechol groups of TA after binding with PBA (Fig. 2b). Consistent with the above results, the concentration of PTNG was proportional to the inhibition of free radicals (Fig. S2b<sup>†</sup>). Last, to focus only on H<sub>2</sub>O<sub>2</sub>, we assessed H<sub>2</sub>O<sub>2</sub>-scavenging ability of PTNG by non-HRP-based H<sub>2</sub>O<sub>2</sub> assay. Due to the formation of the phenylboronic ester group, PTNG significantly reduced H<sub>2</sub>O<sub>2</sub> levels, more than the capability of pPBA, showing increased scavenging ability with an increase in the concentration. Also noteworthy is that there was a negligible scavenging effect of TA against H<sub>2</sub>O<sub>2</sub> (Fig. 2c and S2c<sup>†</sup>). Taken together, these results prove the potential of our PTNG as a strong ROS scavenger to reduce various ROS, including free radicals and H<sub>2</sub>O<sub>2</sub>, based on combined scavenging effects from components of PTNG, which are H<sub>2</sub>O<sub>2</sub>-scavenging phenylboronic ester and radical scavenging TA.

### 3.3 *In vitro* anti-inflammatory effect of PTNG

It is widely known that generation of ROS or RNS accelerates the process of inflammation because ROS or RNS itself can be exploited as a signal molecule of the inflammatory response.<sup>31</sup> Accordingly, our group has reported that scavenging nitric oxide (NO) can alleviate the inflammation in *in vitro* and *in vivo* arthritis models.<sup>32</sup> Since our nanogel exhibited superior antioxidant effects in comparison with each component, pPBA or TA, we thus expected PTNG to act as an alternative anti-inflammatory agent. Prior to demonstration of the therapeutic effect, we evaluated the toxicity of the nanogel *in vitro* by treatment against murine macrophage (RAW264.7) and colon cancer (CT-26 cell line). As shown in Fig. S3,<sup>†</sup> all of the com-

ponents exhibited over 80% of viability even at [PBA] = 200  $\mu$ M, meaning that our PTNG is highly biocompatible.

Next, the anti-inflammatory effect of PTNG was evaluated by the stimulation of RAW264.7 cells with phorbol 12-myristate 13-acetate (PMA), an inflammation activator.<sup>33,34</sup> In brief, extracellular total ROS were quantified by Amplex<sup>®</sup> Red assay, whereas intracellular ROS were evaluated by DCF-DA fluorescence. Moreover, the *in vitro* levels of TNF- $\alpha$  and IL-6, representative pro-inflammatory cytokines, were evaluated by ELISA. For treatment of PMA – although the cytotoxicity of PMA was negligible over a broad range – we chose 200 ng mL<sup>-1</sup> as the model dose for further studies (Fig. S4<sup>†</sup>).<sup>35</sup> The intracellular and extracellular ROS levels were significantly increased when stimulated by PMA, whereas that of the PTNG-treated group was comparable with that of the non-stimulated group (Fig. 3a–c). Interestingly, the intracellular ROS level from TA-treated group, examined by fluorescence of DCF-DA, was relatively lower than that of pPBA-treated group (Fig. 3a and b). We believe that the much lower molecular weight of TA might affect facile uptake of an antioxidant, resulting in a different level of intracellular ROS level. The strongest antioxidant effect of PTNG can be explained by favorable uptake of the more particle-like structured PTNG compared with that of the linearly entangled pPBA.<sup>22,23</sup> Similar to the intracellular ROS level, degree of inflammation, determined by pro-inflammatory cytokines (TNF- $\alpha$ , IL-6), was most alleviated by treatment with PTNG (Fig. 3d and e).

Not only direct stimulation of macrophages with PMA but also elevated levels of extracellular ROS, *i.e.* H<sub>2</sub>O<sub>2</sub>, induce acute inflammation because ROS itself is a signal molecule of the inflammatory response.<sup>36</sup> We therefore postulated that successful scavenging of extracellular ROS may prevent the inflammatory response. A viability test evaluated in the 0–1000  $\mu$ M H<sub>2</sub>O<sub>2</sub> range showed severe toxicity at high concentration, so we selected 200  $\mu$ M H<sub>2</sub>O<sub>2</sub>, which represented around 50% viability as a model ROS level (Fig. S5<sup>†</sup>). First, we studied the effect of ROS scavengers on viability. Briefly, 0–200  $\mu$ M [PBA] of pPBA, TA, or PTNG was treated with 200  $\mu$ M H<sub>2</sub>O<sub>2</sub> against the RAW 264.7 cell line, and viability was measured by MTT assay. Similar to the ROS scavenging property, PTNG had the highest protection ability against ROS-induced cell toxicity among the

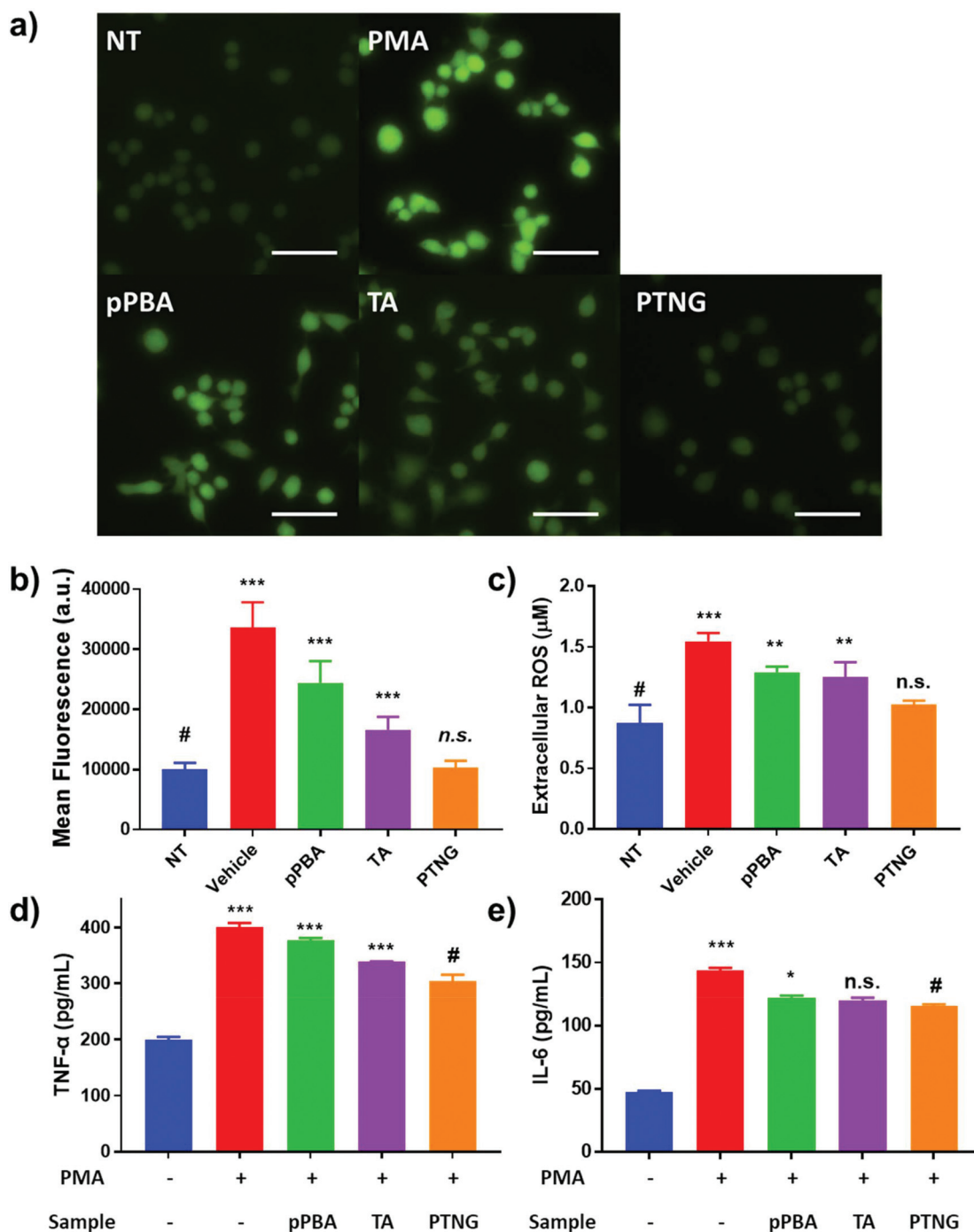


**Fig. 3** Investigation of ROS scavenging effects *in vitro* after PMA treatment. (a) Fluorescence images of RAW 264.7 cells (scale bar = 25  $\mu$ m) after staining with ROS-responsive dye (DCF-DA) and their (b) ROI quantification. (c) Extracellular ROS level and (d and e) pro-inflammatory cytokine levels (TNF- $\alpha$ , IL-6) of RAW 264.7 cells ( $n = 3$ , mean  $\pm$  SD, # compared with other groups, \* $p < 0.05$ , \*\* $p < 0.01$ , \*\*\* $p < 0.001$ ).

other samples (Fig. S6†). Second, the extra- and intracellular ROS levels were quantified by the same methods as that used for PMA-induced acute inflammation. Our PTNG showed the strongest ROS scavenging effect; interestingly, pPBA was much stronger than TA, inconsistent with PMA study (Fig. 4a and b). Nevertheless, the result can be explained by the unique scavenging properties of TA or pPBA against different ROS species. As

mentioned in the various ROS quantification assays, catechol-containing TA was not an effective scavenger against free H<sub>2</sub>O<sub>2</sub>, whereas pPBA or PTNG was.<sup>37,38</sup> Consequently, extracellular ROS was not effectively eliminated by TA, resulting in higher remaining extracellular and intracellular ROS levels (Fig. 4c). In the case of inflammation, the level of cytokine was not significantly different between the samples, which could have

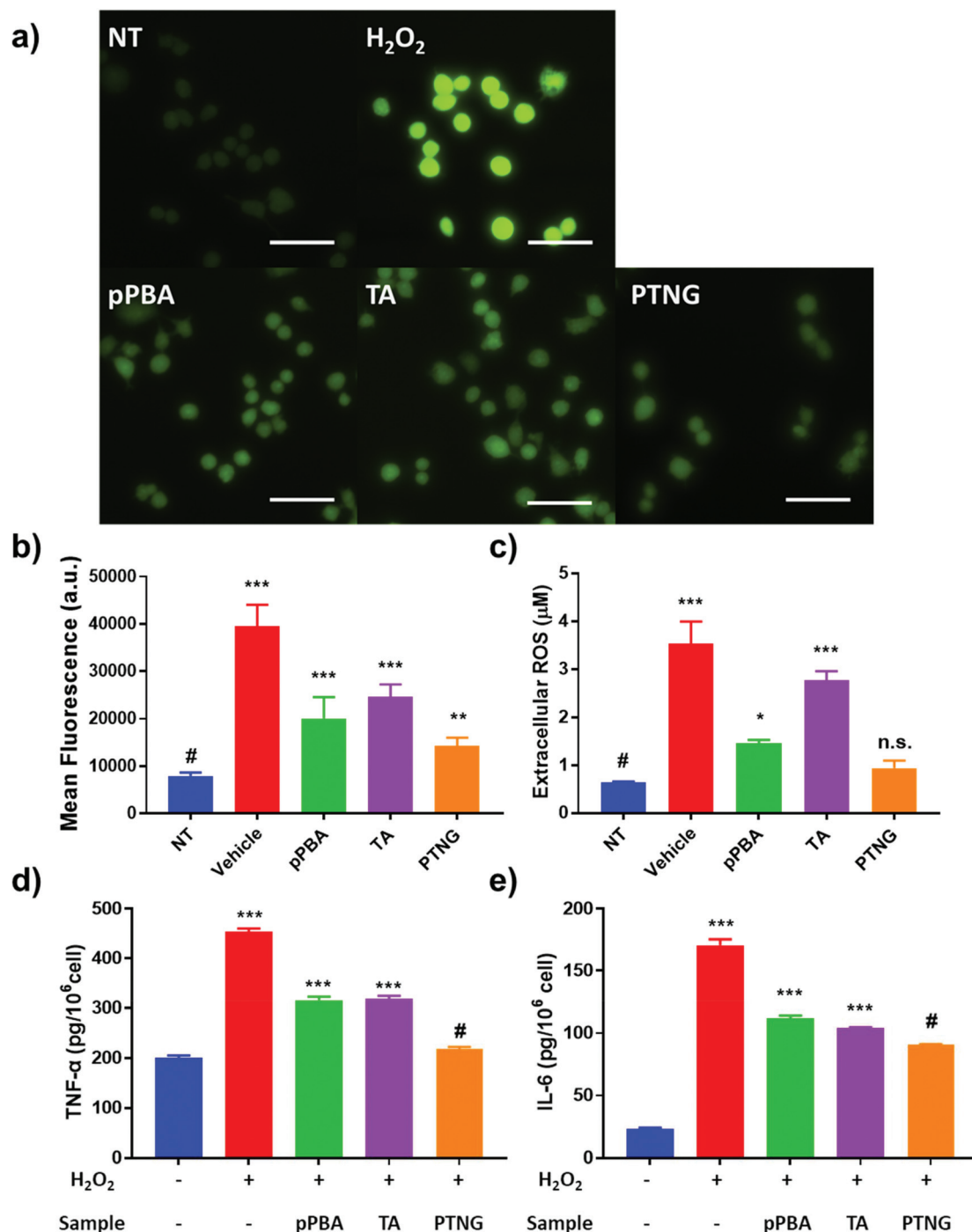


**Fig. 4** Investigation of ROS scavenging effects *in vitro* after 200  $\mu\text{M}$   $\text{H}_2\text{O}_2$  treatment. (a) Fluorescence images of RAW 264.7 cells (scale bar = 25  $\mu\text{m}$ ) after staining with ROS-responsive dye (DCF-DA) and their (b) ROI quantification. (c) Extracellular ROS level of RAW 264.7 cells. (d and e) Pro-inflammatory cytokine levels (TNF- $\alpha$ , IL-6) of RAW 264.7 cells, compensated with viability ( $n = 3$ , mean  $\pm$  SD, # compared with other groups, \* $p < 0.05$ , \*\* $p < 0.01$ , \*\*\* $p < 0.001$ ).

been caused by differing viability at each condition (Fig. S5b and S7†). After compensation with viability under the same conditions, inflammatory cytokine level per  $\text{H}_2\text{O}_2$ -treated cell was significantly reduced by PTNG (Fig. 4d and e).

Taken together, we demonstrated an outstanding ROS scavenging effect of phenylboronic ester-based PTNG *in vitro*

under intracellular (PMA) or extracellular ( $\text{H}_2\text{O}_2$ ) ROS generation. TA was not an effective scavenger against  $\text{H}_2\text{O}_2$  *in vitro*, as observed in previous ROS scavenging assays. Moreover, effective scavenging of cellular ROS was highly correlated with pro-inflammatory cytokines including IL-6 and TNF- $\alpha$ . Therefore, our findings strongly suggest that a ROS scavenger



such as PTNG can be exploited as an alternative anti-inflammatory agent for the treatment of inflammatory diseases.

### 3.4 *In vivo* anti-inflammatory effect of PTNG

In accordance with our previous results, an excellent anti-inflammatory effect of PTNG derived from its ROS scavenging property, we further examined PTNG for treating inflammatory disease. Prior to administration, *in vivo* biocompatibility of our materials was confirmed by hemolysis assay (Fig. S8†). Negligible hemolysis was observed for all materials except TA, which exhibited some proportion of hemolytic property (~10%), which might be derived from strong interaction between the catechol group and the membrane of erythrocytes.<sup>39</sup> Before therapeutic evaluation, biodistribution of PTNG was also monitored by *in vivo* fluorescence image to ensure

that nanogel sufficiently remains in peritoneum to show anti-inflammatory effect. In similar with therapeutic evaluation *in vivo*, we used the zymosan-induced acute peritonitis (ZIP) model.<sup>40</sup> Briefly, zymosan was administrated intraperitoneally (i.p.), followed by i.p. injection of our materials after 1 h to monitor the biodistribution. Fortunately, peritoneal distribution of PTNG was observed for at least 4 h, whereas clearance through hepatic pathway was clearly occurred in 48 h (Fig. S9†).<sup>41,42</sup> Encouraged from biodistribution results, we finally evaluated therapeutic effect of PTNG as an anti-inflammatory agent *in vivo*. After 5 h post-administration of our materials in ZIP model, the peritoneal cavity was washed with saline to analyze the cytokines in peritoneal lavage and recruited inflammatory cells; serum was also collected to measure the level of whole-body inflammation (Fig. 5a). As

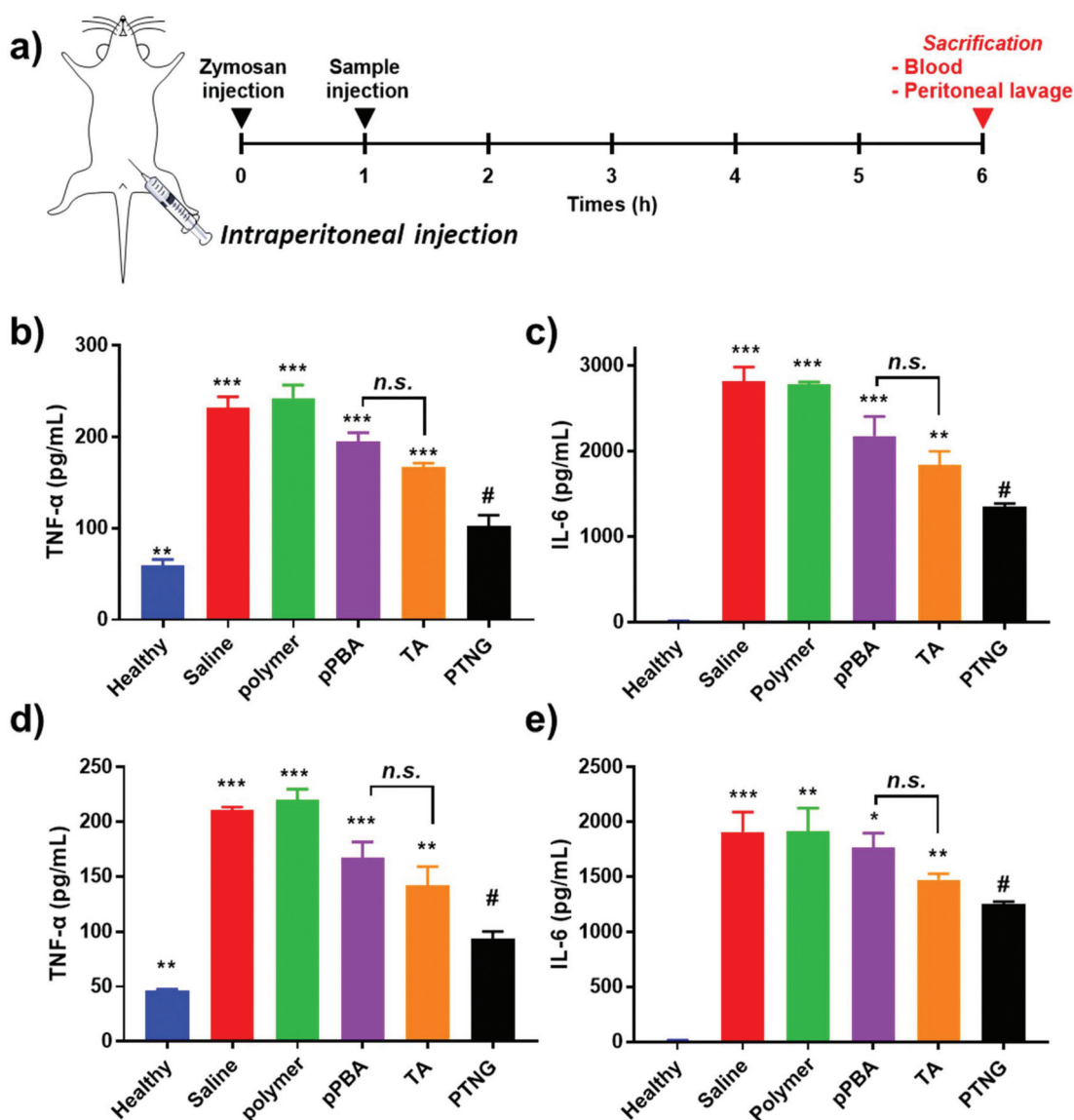
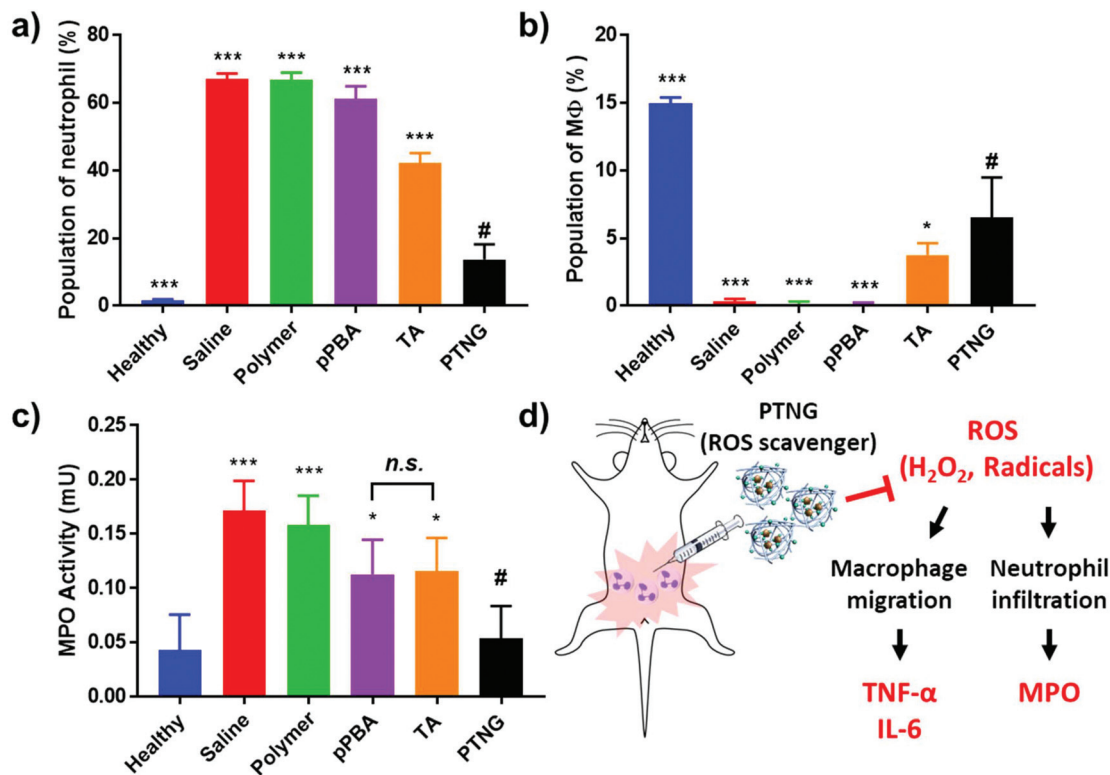


Fig. 5 *In vivo* therapeutic model of PTNG for treatment of zymosan-induced peritonitis (ZIP). (a) Overall experimental timeline for ZIP mouse model. Quantification of pro-inflammatory cytokines including (b) TNF- $\alpha$  and (c) IL-6 in the peritoneal lavage and (d) TNF- $\alpha$  and (e) IL-6 in the serum, ( $n = 3$ , mean  $\pm$  SD, # compared with sample groups, \* $p < 0.05$ , \*\* $p < 0.01$ , \*\*\* $p < 0.001$ ).



**Fig. 6** Study of anti-inflammatory effects in zymosan-induced peritonitis mouse model. (a and b) Flow-cytometric analysis of (a) neutrophil and (b) residual peritoneal macrophages, and (c) MPO activity of peritoneal lavage ( $n = 3$ , mean  $\pm$  SD, # compared with sample groups, \* $p < 0.05$ , \*\* $p < 0.01$ , \*\*\* $p < 0.005$ ). (d) Schematic for anti-inflammatory mechanism of PTNG.

was done in the cellular study, the pro-inflammatory cytokine level of both peritoneal lavage and serum showed quite obvious zymosan-induced acute inflammation. In contrast, PTNG significantly reduced the level of inflammation (Fig. 5b–e).<sup>43,44</sup> The components of PTNG including pPBA and TA also declined inflammation to some degree, but the difference between them was not significant. Moreover, the number of recruited peritoneal cells, standing for level of inflammation, showed a similar tendency with cytokine levels (Fig. S10†). Nonetheless, not only the number but also the type of recruited cell is another important criterion to estimate the level of inflammation; thus, the population of recruited cells was analyzed by flow cytometry. As shown in Fig. 6a, the population of neutrophils was greatly increased by challenging with zymosan, and treatment by antioxidants reduced a certain level of infiltrated neutrophils (CD11b<sup>high</sup>/Ly6G<sup>high</sup>), as would be expected.<sup>45</sup> Interestingly, the population of peritoneal macrophage (CD11b<sup>high</sup>/F4/80<sup>high</sup>) showed a reversed tendency; several studies have shown that the population of resident macrophages (large peritoneal macrophage, LPM) is greatly decreased in the case of inflammation, which might be caused by their movement into lymph nodes (Fig. 6b).<sup>46–48</sup> Therefore, we believe that scavenging the ROS prevented an initial activation of residual macrophages, followed by the inhibition of chemotaxis-mediated recruitment of neutrophils and inflammatory monocytes/macrophage, as revealed by

results of flow cytometry and local and systemic pro-inflammatory cytokine levels. An activity value of myeloperoxidase (MPO), a representative marker of active neutrophils, showed a similar tendency in accordance with the neutrophil population, implying the inhibition of neutrophils after treatment with antioxidants (Fig. 6c).<sup>49,50</sup> In addition, there was no significant toxicity observed by histological analysis with H&E staining of major organs and peritoneum (Fig. S11†). Taken together, our ROS-responsive PTNG can be utilized as an anti-inflammatory agent by itself, derived from its strong ROS scavenging capability (Fig. 6d).

## 4. Conclusion

In this study, we reported a facile preparation of biocompatible antioxidants. By mixing polymeric phenylboronic acid with tannic acid, a natural antioxidant, our nanogel (PTNG) was easily produced by the formation of phenylboronic ester with innate H<sub>2</sub>O<sub>2</sub> responsiveness. Due to the high reactivity of phenylboronic ester as well as the inherent radical scavenger TA, PTNG exhibited superior ROS scavenging behavior in comparison with the components. Effective scavenging of ROS successfully reduced inflammation of macrophages induced by PMA or external ROS, as revealed by the internal ROS and pro-inflammatory cytokine level. Furthermore, PTNG was treated

in zymosan-induced peritonitis model mice, and change of pro-inflammatory cytokine levels in serum, in peritoneal lavage, and in peritoneal cell population indicated a significant alleviation of induced inflammation *in vivo*. In conclusion, we strongly believe that our study has provided an alternative approach for the treatment of inflammatory diseases by scavenging overproduced ROS.

## Conflicts of interest

There are no conflicts to declare.

## Acknowledgements

This research was supported by the National Research Foundation of Korea (NRF) grant (NRF-2017R1E1A1A01074088), Bio & Medical Technology Development Program (NRF-2017M3A9F5030930), and Creative Materials Discovery Program (NRF-2018M3D1A1058813) funded by the Korea government (Ministry of Science and ICT). J. Yeo was supported by Global Ph. D. Fellowship Program funded by the Ministry of Education (NRF-2017-H1A2A1045572).

## References

- 1 R. H. Burdon, *Biochem. Soc. Trans.*, 1996, **24**, 1028–1032.
- 2 T. Finkel, *J. Cell Biol.*, 2011, **194**, 7–15.
- 3 M. A. Torres, J. D. Jones and J. L. Dangel, *Plant Physiol.*, 2006, **141**, 373–378.
- 4 M. Schieber and N. S. Chandel, *Curr. Biol.*, 2014, **24**, R453–R462.
- 5 V. Afonso, R. Champy, D. Mitrovic, P. Collin and A. Lomri, *Jt., Bone, Spine*, 2007, **74**, 324–329.
- 6 B. Halliwell, *Br. J. Exp. Pathol.*, 1989, **70**, 737–757.
- 7 P. H. Chan, *J. Cereb. Blood Flow Metab.*, 2001, **21**, 2–14.
- 8 G. Waris and H. Ahsan, *J. Carcinog.*, 2006, **5**, 14.
- 9 A. Bast and G. R. M. M. Haenen, *Environ. Toxicol. Pharmacol.*, 2002, **11**, 251–258.
- 10 B. Halliwell, *Lancet*, 2000, **355**, 1179–1180.
- 11 H. Kappus and A. T. Diplock, *Free Radicals Biol. Med.*, 1992, **13**, 55–74.
- 12 A. R. Ndhlala, M. Moyo and J. Van Staden, *Molecules*, 2010, **15**, 6905–6930.
- 13 M. L. Urso and P. M. Clarkson, *Toxicology*, 2003, **189**, 41–54.
- 14 R. I. M. van Haften, C. T. A. Evelo, G. R. M. M. Haenen and A. Bast, *Biochem. Biophys. Res. Commun.*, 2001, **280**, 631–633.
- 15 H. J. Kwon, D. Kim, K. Seo, Y. G. Kim, S. I. Han, T. Kang, M. Soh and T. Hyeon, *Angew. Chem., Int. Ed.*, 2018, **57**, 9408–9412.
- 16 J. Yao, Y. Cheng, M. Zhou, S. Zhao, S. Lin, X. Wang, J. Wu, S. Li and H. Wei, *Chem. Sci.*, 2018, **9**, 2927–2933.
- 17 M. Kumari, S. P. Singh, S. Chinde, M. F. Rahman, M. Mahboob and P. Grover, *Int. J. Toxicol.*, 2014, **33**, 86–97.
- 18 W. Lin, Y. W. Huang, X. D. Zhou and Y. Ma, *Int. J. Toxicol.*, 2006, **25**, 451–457.
- 19 E. J. Park, J. Choi, Y. K. Park and K. Park, *Toxicology*, 2008, **245**, 90–100.
- 20 A. M. Schrand, M. F. Rahman, S. M. Hussain, J. J. Schlager, D. A. Smith and A. F. Syed, *Wiley Interdiscip. Rev.: Nanomed. Nanobiotechnol.*, 2010, **2**, 544–568.
- 21 Q. Zhang, F. Zhang, Y. Chen, Y. Dou, H. Tao, D. Zhang, R. Wang, X. Li and J. Zhang, *Chem. Mater.*, 2017, **29**, 8221–8238.
- 22 J. Lee, J. Kim, Y. M. Lee, D. Park, S. Im, E. H. Song, H. Park and W. J. Kim, *Acta Pharmacol. Sin.*, 2017, **38**, 848–858.
- 23 İ. Gülçin, Z. Huyut, M. Elmastaş and H. Y. Aboul-Enein, *Arabian J. Chem.*, 2010, **3**, 43–53.
- 24 S. Nam, D. M. Smith and Q. P. Dou, *Cancer Epidemiol. Biomarkers Prev.*, 2001, **10**, 1083–1088.
- 25 M. L. Mota, G. Thomas and J. M. Barbosa Filho, *J. Ethnopharmacol.*, 1985, **13**, 289–300.
- 26 B. Zhou, X. Hu, J. Zhu, Z. Wang, X. Wang and M. Wang, *Int. J. Biol. Macromol.*, 2016, **91**, 68–74.
- 27 Q. Xu, C. He, C. Xiao and X. Chen, *Macromol. Biosci.*, 2016, **16**, 635–646.
- 28 T. Zhang, X. Chen, C. Xiao, X. Zhuang and X. Chen, *Polym. Chem.*, 2017, **8**, 6209–6216.
- 29 A. C. Sedgwick, H. H. Han, J. E. Gardiner, S. D. Bull, X. P. He and T. D. James, *Chem. Commun.*, 2017, **53**, 12822–12825.
- 30 G. I. Berglund, G. H. Carlsson, A. T. Smith, H. Szöke, A. Henriksen and J. Hajdu, *Nature*, 2002, **417**, 463–468.
- 31 L. Fialkow, Y. Wang and G. P. Downey, *Free Radicals Biol. Med.*, 2007, **42**, 153–164.
- 32 J. Yeo, Y. M. Lee, J. Lee, D. Park, K. Kim, J. Kim, J. Park and W. J. Kim, *Nano Lett.*, 2019, **19**, 6716–6724.
- 33 K. Zhao, Z. Huang, L. Hongling, J. Zhou and T. Wei, *Biosci. Rep.*, 2009, **30**, 233–241.
- 34 E. J. Swindle, J. A. Hunt and J. W. Coleman, *J. Immunol.*, 2002, **169**, 5866.
- 35 J. N. Gibson, P. Beesetty, C. Sulentic and J. A. Kozak, *J. Visualized Exp.*, 2016, e55212, DOI: 10.3791/55212.
- 36 A. van der Vliet and Y. M. W. Janssen-Heininger, *J. Cell. Biochem.*, 2014, **115**, 427–435.
- 37 N. Bensalah, K. Chair and A. Bedoui, *Sustainable Environ. Res.*, 2018, **28**, 1–11.
- 38 S. Ji-min, L. Xue-yan, C. Zhong-lin, G. Xiao-hong, Z. Xue and X. Zhen-zhen, *Water Sci. Technol.*, 2008, **57**, 2043–2050.
- 39 W. G. La, S. H. Bhang, J. Y. Shin, H. H. Yoon, J. Park, H. S. Yang, S. H. Yu, Y. E. Sung and B. S. Kim, *Biotechnol. Prog.*, 2012, **28**, 1055–1060.
- 40 J. L. Cash, G. E. White and D. R. Greaves, in *Methods in Enzymology*, Academic Press, 2009, vol. 461, pp. 379–396.
- 41 F. Alexis, E. Pridgen, L. K. Molnar and O. C. Farokhzad, *Mol. Pharmaceutics*, 2008, **54**, 505–515.
- 42 M. R. Longmire, M. Ogawa, P. L. Choyke and H. Kobayashi, *Bioconjugate Chem.*, 2011, **22**, 993–1000.

- 43 R. Watzlawick, E. E. Kenngott, F. D. Liu, J. M. Schwab and A. Hamann, *PLoS One*, 2015, **10**, e0137651.
- 44 S. Niu, Z. Bian, A. Tremblay, Y. Luo, K. Kidder, A. Mansour, K. Zen and Y. Liu, *J. Immunol.*, 2016, **197**, 3293–3301.
- 45 M. Takahashi, K. Izawa, M. Urai, Y. Yamanishi, A. Maehara, M. Isobe, T. Matsukawa, A. Kaitani, A. Takamori, S. Uchida, H. Yamada, M. Nagamine, T. Ando, T. Shimizu, H. Ogawa, K. Okumura, Y. Kinjo, T. Kitamura and J. Kitaura, *Sci. Signaling*, 2019, **12**, eaar5514.
- 46 G. J. Bellingan, P. Xu, H. Cooksley, H. Cauldwell, A. Shock, S. Bottoms, C. Haslett, S. E. Mutsaers and G. J. Laurent, *J. Exp. Med.*, 2002, **196**, 1515.
- 47 M. Dosch, J. Zindel, F. Jebbawi, N. Melin, D. Sanchez-Taltavull, D. Stroka, D. Candinas and G. Beldi, *eLife*, 2019, **8**, e42670.
- 48 E. E. B. Ghosn, A. A. Cassado, G. R. Govoni, T. Fukuhara, Y. Yang, D. M. Monack, K. R. Bortoluci, S. R. Almeida, L. A. Herzenberg and L. A. Herzenberg, *Proc. Natl. Acad. Sci. U. S. A.*, 2010, **107**, 2568–2573.
- 49 Y. Hori, Y. Nihei, Y. Kurokawa, A. Kuramasu, Y. Makabe-Kobayashi, T. Terui, H. Doi, S. Satomi, E. Sakurai, A. Nagy, T. Watanabe and H. Ohtsu, *J. Immunol.*, 2002, **169**, 1978–1983.
- 50 B. Pulli, M. Ali, R. Forghani, S. Schob, K. L. Hsieh, G. Wojtkiewicz, J. J. Linnoila and J. W. Chen, *PLoS One*, 2013, **8**, e67976.